

Nonresonant Raman spectrum in infinite and finite single-wall carbon nanotubes

A. Rahmani,^{1,2} J.-L. Sauvajol,¹ S. Rols,³ and C. Benoit¹

¹*Groupe de Dynamique des Phases Condensées (UMR CNRS 5581), Université Montpellier II, 34095 Montpellier Cedex 5, France*

²*Département de Physique, Université MY Ismail, Faculté des Sciences, Boîte Postal 4010, 50000 Meknès, Morocco*

³*Spallation Neutron Source Argonne National Laboratory, Argonne 60439-4814*

(Received 19 February 2002; revised manuscript received 28 June 2002; published 6 September 2002)

We use the spectral moments method in the framework of the bond-polarization theory to calculate polarized nonresonant Raman spectra of chiral and achiral single-wall carbon nanotubes as a function of their diameter and length. In a previous approach, an investigation of finite-size effects was limited to a narrow length range (below 50 Å). The present work extends the analysis to a larger range of finite lengths (from 20 to 850 Å) as well as to achiral and chiral tubes of different diameters.

DOI: 10.1103/PhysRevB.66.125404

PACS number(s): 63.22.+m, 78.30.Na

I. INTRODUCTION

Resonant Raman spectroscopy has provided a powerful tool for the observation of diameter-selective phonon modes of single-wall carbon nanotubes (SWNT's). The Raman spectrum of SWNT's is dominated by $A(A_{1g})$ radial breathing modes (RBM) below 400 cm^{-1} , and by tangential modes (TM) in the high-frequency region ($1400\text{--}1600\text{ cm}^{-1}$). The latter consist of two A , two E_1 and two E_2 phonon modes for chiral nanotubes, and one A_{1g} , one E_{1g} , and one E_{2g} mode for achiral (armchair and zigzag) nanotubes.¹ It was found that the RBM frequency closely depends on the diameter of the tubes, regardless of their chirality.² The TM shape, however, depends strongly on whether the tube is metallic or semiconducting. More precisely, TM Raman scattering from metallic SWNT's shows a broad component, whose envelope is well described by a Breit-Wigner-Fano line shape.^{3–5} By contrast to the tremendous number of Raman studies in the RBM- and TM-frequency range, studies on the intermediate-frequency range ($600\text{--}1300\text{ cm}^{-1}$) have been restricted to a few experimental^{6,7} and theoretical⁸ works. A nonzero intensity was predicted for nanotubes with a finite length only, and experimentally the Raman intensity is weak in this frequency range. However, one can resolve several peaks whose assignment is still a matter of controversy. Recently, distinct characteristic spectra were identified in the intermediate-frequency range, with each spectrum featured by a couple of lines composed of one first-order mode and one subtractive combination band, both exhibiting a strong excitation dependence. The origin of such a behavior remains an open question.⁹

Polarized Raman spectroscopy on aligned SWNT's was only recently reported.^{10–14} Most experimental studies show a simple intensity dependence of the signal: both the RBM and TM intensities peak at a maximum when the light is polarized along the tube axis, and are significantly reduced when the light (either incident or scattered) is polarized perpendicular to the tube axis.^{10–12} By contrast, a symmetry selection was reported in polarized Raman spectroscopy on aligned multiwalled carbon nanotubes¹³ (MWNT's) and semiconducting SWNT's bundles.¹⁴ Close agreement between nonresonant-theory-based calculations and experimental observations was obtained for TM intensities in MWNT's

which exhibit a minimum for $\theta=55^\circ$ in parallel/parallel configuration (θ denotes the angle between the polarization and the tube axis).¹³ For SWNT's bundles, the TM bunch of tangential modes was separated into four intrinsic components with the following symmetry assignment:¹⁴ 1549 cm^{-1} [$E_2(E_{2g})$], 1567 cm^{-1} [$A(A_{1g})$]+ $E_1(E_{1g})$], 1590 cm^{-1} [$A(A_{1g})$]+ $E_1(E_{1g})$] and 1607 cm^{-1} $E_2(E_{2g})$. In the latter study, the relative intensity of the different modes was successfully explained by symmetry-based considerations of a (10,10) nanotube.² In order to gain more insight into these questions, we calculated the dependence of the nonresonant polarized Raman spectrum of achiral and chiral single-wall carbon nanotubes as a function of the diameter and length of the tubes. Raman spectra were calculated using the spectral moments method.

II. COMPUTATIONAL METHOD

The moments method was initially developed by different authors for studying electronic properties in solid-state physics.^{15,16} A few years ago, the spectral moments method (SMM) was shown to be a powerful tool for determining infrared absorption, Raman scattering, and inelastic neutron-scattering spectra of harmonic systems.^{17–20} This method can be applied to very large systems, whatever the type of atomic forces, the spatial dimension, and structure of the material. This method was previously used to study the dynamical properties of different disordered systems having more than 10^6 degrees of freedom, as is the case for Sierpinski gaskets,¹⁸ diffusion-limited cluster-cluster aggregates¹⁹ and silica aerogels.²⁰

The time-averaged power flux of the Raman-scattered light in a given direction, with a frequency between ω_f and $\omega_f+d\omega_f$ in a solid angle $d\Omega$, is related to the differential scattering cross section,

$$\frac{d^2\sigma}{d\Omega d\omega_f} = \frac{1}{8\pi^2 c^2} \omega_f^3 \omega_i [B(\omega) + 1] \hbar \times \sum_{\alpha\beta\gamma\lambda} v_\alpha v_\beta H_{\alpha\gamma\beta\lambda}(\omega) w_\gamma w_\lambda, \quad (1)$$

where

$$H_{\alpha\gamma\beta\lambda}(\omega) = \sum_j a_{\alpha\gamma}^*(j) a_{\beta\lambda}(j) \frac{1}{2\omega_j} [\delta(\omega - \omega_j) - \delta(\omega + \omega_j)], \quad (2)$$

with

$$a_{\alpha\gamma}(j) = \sum_{n\delta} \frac{\pi_{\alpha\gamma,\delta}^n}{\sqrt{M_n}} \langle \delta n | j \rangle, \quad (3)$$

ω_j is the frequency of the incident light, \vec{v} and \vec{w} are the polarization unit vectors for scattered and incident light respectively, $B(\omega)$ is the Bose factor, M_n the mass of the n th atom, ω_j and $\langle \delta n | j \rangle$ are the frequency and (δn) component of the j th mode. The coefficients $\pi_{\alpha\gamma,\delta}^n$ connect the polarization fluctuations to the atomic motions²¹ and they are obtained by expanding the polarizability tensor $\tilde{\pi}^n$ in terms of atom displacements u_δ^n , with

$$\pi_{\alpha\gamma,\delta}^n = \sum_m \left(\frac{\partial \pi_{\alpha\gamma}^m}{\partial u_\delta^n} \right)_0, \quad (4)$$

A usual method to calculate the Raman spectrum involves injecting in the previous expressions the values of ω_j and $\langle \delta n | j \rangle$ obtained by solving the equation

$$\tilde{D} | j \rangle = \omega_j^2 | j \rangle, \quad (5)$$

where \tilde{D} is the dynamical matrix of the system, with the element $D_{\alpha\beta}(nm) = \langle \alpha n | \tilde{D} | \beta m \rangle$.

When the system contains a large number of atoms, as for long finite nanotubes, the dynamical matrix \tilde{D} is very large and its diagonalization fails or requires long computing time. In contrast, the spectral moments method allows us to directly compute the Raman spectrum of very large harmonic systems without any diagonalization of the dynamical matrix.¹⁷ In order to test the spectral moments method, Raman spectra for different systems of limited sizes were calculated by a direct diagonalization of the dynamical matrix, and we have stated that these latter spectra and those obtained from the spectral moments method were exactly the same.^{18,22}

Considering the symmetrical function $I(\omega)$ where $a(j)$ is given by Eq. (3),

$$I(\omega) = \sum_j \frac{|a(j)|^2}{2\omega_j} [\delta(\omega - \omega_j) + \delta(\omega + \omega_j)]. \quad (6)$$

This function is identical (for $\omega > 0$), apart from a constant and the Bose factor, to a component of the Raman-scattering cross section, [Eq. (1)], for a given polarization of the incident and scattered lights. The response of the system is given by the function $I(\omega)$, which can be further written as

$$J(u) = \sum_j |a(j)|^2 \delta(u - \lambda_j), \quad (7)$$

where, $u = \omega^2$ and $\lambda_j = \omega_j^2$.

$J(u)$ can be directly carried out from the dynamical matrix, \tilde{D} , and from the polarizability tensor, without any diagonalization. Indeed, it is easy to show that

$$J(u) = -(1/\pi) \lim_{\epsilon \rightarrow 0^+} \text{Im}[R(z)], \quad (8)$$

where $z = u + i\epsilon$ and $R(z) = \langle q | (z\tilde{I} - \tilde{D})^{-1} | q \rangle$.

The (δn) component of the $|q\rangle$ vector is given by the expression

$$\langle \delta n | q \rangle = \frac{\pi_{\alpha\gamma,\delta}^n}{\sqrt{M_n}}, \quad (9)$$

which is supposedly known. The spectral moments method consists of developing $R(z)$ in a continued fraction

$$R(z) = \frac{b_0}{z - a_1 - b_1/z - a_2 - b_2/z - a_3 - b_3/z \dots}, \quad (10)$$

Coefficients a_n and b_n are obtained from iterations¹⁷ $a_{m+1} = \bar{v}_{mm}/v_{mm}$ and $b_{m+1} = v_{m+1m+1}/v_{mm}$ with $b_0 = 1$, and the generalized moments v_{nn} and \bar{v}_{nn} are given by

$$v_{mm} = \langle q_m | q_m \rangle \quad \text{and} \quad \bar{v}_{mm} = \langle q_m | \tilde{D} | q_m \rangle$$

with $|q_{m+1}\rangle = (\tilde{D} - a_{m+1})|q_m\rangle - b_m|q_{m-1}\rangle, |q_{-1}\rangle = 0$

and $|q_0\rangle = |q\rangle$.

Iterations enable the computation of expression (10) and then the function $I(\omega)$.

Each element of the dynamical matrix, \tilde{D} , is given by

$$D_{\alpha\beta}(n,m) = \frac{1}{\sqrt{M_n M_m}} \phi_{\alpha\beta}(n,m) \quad (11)$$

with $\phi_{\alpha\beta}(n,m)$ being the force constants between n and m atoms. In our calculations, the interactions are restricted only to the first-, second-, third- and fourth-nearest neighbors. So only four (3×3) force-constant matrices are required to generate the dynamical matrix of SWNT.² Using graphite force constants,²³ the force-constant matrix between the n and m carbon atoms is given by rotating the chemical bond from the two-dimensional plane of graphite to the three-dimensional cylindrical coordinate system of a nanotube² (see Fig. 1 in Ref. 2 for a definition of the rotations). To take the effect of curvature into account, the force-constant parameters are scaled by formula (6) in Ref. 2.

The Raman intensity is calculated within the nonresonant bond-polarization theory in which bond-polarization parameters are used.²⁴ In this approach, the derivatives $\pi_{\alpha\beta,\gamma}^n$ are given by

$$\begin{aligned} \pi_{\alpha\beta,\gamma}^n = & \sum_m \frac{1}{3} (2\alpha'_p + \alpha'_l) \delta_{\alpha\beta} \hat{r}_\gamma + (\alpha'_l - \alpha'_p) \left(\hat{r}_\alpha \hat{r}_\beta - \frac{1}{3} \delta_{\alpha\beta} \right) \\ & \times \hat{r}_\gamma + \frac{(\alpha_l - \alpha_p)}{r} (\delta_{\alpha\gamma} \hat{r}_\beta + \delta_{\beta\gamma} \hat{r}_\alpha - 2\hat{r}_\alpha \hat{r}_\beta \hat{r}_\gamma), \quad (12) \end{aligned}$$

where \hat{r} is the unit vector along vector r that connects the n and m atoms linked by the bond, $\alpha'_l = (\partial\alpha_l/\partial r)_0$ and $\alpha'_p = (\partial\alpha_p/\partial r)_0$.

Parameters α_l and α_p correspond to the longitudinal and perpendicular bond polarizability, respectively. In SWNT's, a single type of bond occurs and the bond polarizability model is completely defined by three parameters: $\alpha = 2\alpha'_p + \alpha'_l$, $\beta = \alpha'_l - \alpha'_p$, and $\gamma = \alpha_l - \alpha_p$. The empirical parameters used in this study are $\alpha = 4.7 \text{ \AA}^2$, $\beta = 4.0 \text{ \AA}^2$, and $\gamma = 0.04 \text{ \AA}^3$ (Ref. 2).

III. RESULTS AND DISCUSSION

Here we report calculations for polarized Raman spectra of achiral and chiral SWNT's of different diameters and lengths performed using the spectral moments method. The mode frequency is directly obtained from the position of the peak in the calculated Raman spectrum. The line shape of each peak is assumed to be Lorentzian and the linewidth is fixed at 1.7 cm^{-1} . For each SWNT, the intensities of the different polarized spectra are normalized and can be compared. For clarity, the peaks with an intensity of less than 10^{-3} times the intensity of the $A(A_{1g})$ tangential mode were not displayed in the figures. In all our calculations, the nanotube axis is along the Z axis and a carbon atom is along the X axis of the nanotube reference frame. For θ_x and $\theta_y = 0^\circ$ (see text), the Z nanotube axis is along the z axis and the X nanotube axis is along the x axis of the laboratory reference frame. The laser beam is kept along the y axis. In the VV configuration, both the incident and scattered polarizations are along the z axis and, for the VH configuration, the incident and scattered polarizations are along the z and x axes respectively.

A. Polarized Raman spectra of infinite crystals of SWNT's

First, we calculated polarized Raman spectra for achiral (armchair and zigzag) and chiral infinite crystal of nanotubes with different diameters. For the infinite crystal of nanotubes, calculations are performed by applying periodic conditions on unit cells. For infinite tubes, we can compare spectra calculated by the spectral moments method with those calculated by the direct diagonalization of the dynamical matrix. We state that both approaches lead to exactly the same position and intensity for the different peaks.

(i) Polarized Raman spectra have been obtained in a large diameter range: 0.7–2.5 nm. Obviously, the different behaviors of Raman modes with diameter and chirality, as for instance the dependence of the $A(A_{1g})$ RBM with the inverse of the diameter which was established by different approaches,^{2,25–27} were well reproduced in our calculations. In Fig. 1, an illustration of the dependence of polarized Raman spectra with the chirality is given. The ZZ , ZX and YX Raman spectra of the infinite (10,10), (17,0), and (14,7) SWNT's (tubes with diameters of 1.37 nm, 1.35 nm, and 1.47 nm, respectively) are displayed in the RBM and TM regions. As expected from symmetry considerations,² the TM bunch in the chiral tube spectra shows two peaks for each symmetry as compared to one peak for each symmetry in achiral SWNT's. The vicinity of the calculated frequencies

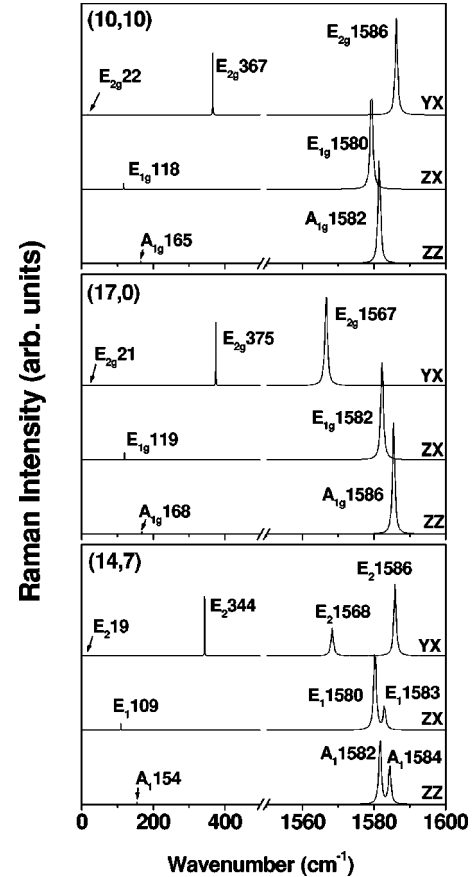


FIG. 1. Polarized Raman spectra of infinite crystals of (10,10) (top), (17,0) (middle), and (14,7) (bottom) SWNT's.

of $A(A_{1g})$ and $E_1(E_{1g})$ tangential modes can be pointed out: A_{1g} , 1582 cm^{-1} and E_{1g} , 1580 cm^{-1} for (10,10) SWNT's; A_{1g} , 1586 cm^{-1} and E_{1g} , 1582 cm^{-1} for (17,0) SWNT's; and A , 1582 cm^{-1} , 1584 cm^{-1} and E_1 , 1580 cm^{-1} , 1583 cm^{-1} for (14,7) SWNT's. These results highlight the difficulty of experimentally resolving $A(A_{1g})$ and $E_1(E_{1g})$ modes, as discussed in Ref.14.

It is generally problematic to match the experimental results with the SMM predictions obtained in the framework of a nonresonance Raman theory. For instance, the calculated intensity of $A(A_{1g})$, $E_1(E_{1g})$, and $E_2(E_{2g})$ TM modes are close (Fig. 1), contrary to the experimental Raman data^{1,3–7}. In resonance Raman spectroscopy, enhancement of the Raman intensity depends on the phonon symmetries²⁸ and thus we do not use the nonresonant predicted relative intensities between the different phonon symmetries in our analysis of the experimental spectra. Nevertheless, these predicted results can be used to interpret the change in intensity for modes with the same symmetry but with different chiralities.²⁹ Finally, the SMM predictions concerning the number and frequency of Raman lines as a function of diameter, length, and chirality do not depend on the resonant process of Raman scattering and the SMM predictions can help to interpret the experimental data.

In the $(600\text{--}1300 \text{ cm}^{-1})$ intermediate-frequency region (not shown), only a weak E_{2g} mode at 865 cm^{-1} , a very weak E_{1g} mode at 868 cm^{-1} , and two very weak E_1 and E_2

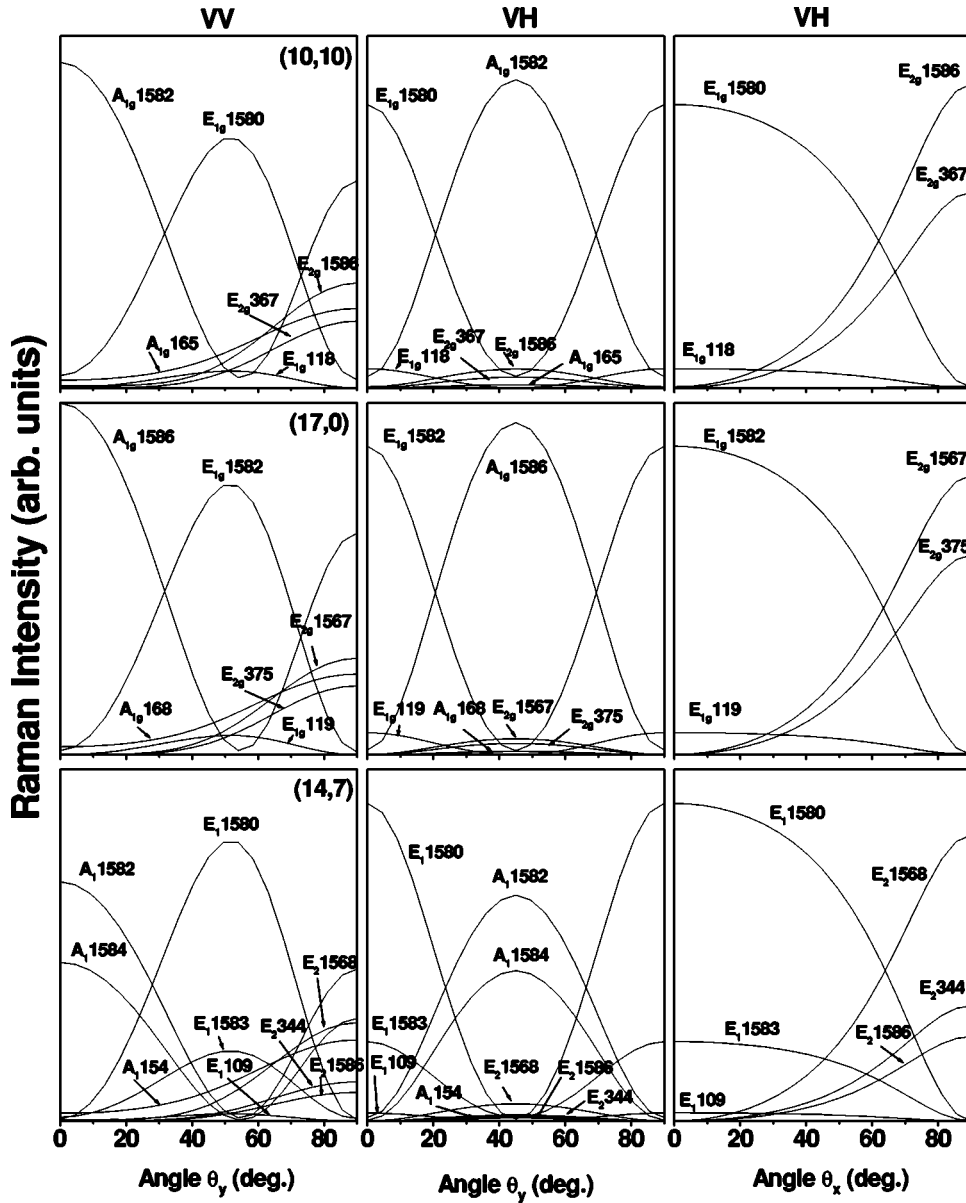


FIG. 2. Raman intensities as a function of the sample orientation for infinite crystals of (10,10) (top), (17,0) (middle), and (14,7) (bottom) SWNT's.

modes at 865 cm^{-1} and 869 cm^{-1} , were calculated for (10,10), (17,0), and (14,7) nanotubes, respectively. In agreement with these results, a mode around 869 cm^{-1} was observed in a large number of Raman spectra.^{6,9} By contrast, these calculations do not predict the presence of the other peaks observed experimentally in the intermediate-frequency range, e.g., the well-defined first-order Raman peaks at 750 cm^{-1} and 780 cm^{-1} that were measured in the Raman spectra of several SWNT samples excited at 2.41 eV .⁹

(ii) The sample orientation dependence of the Raman spectrum was calculated for (10,10), (17,0), and (14,7) SWNT's (Fig. 2). θ_x and θ_y are rotation angles of the nanotube around the x and y axes of the laboratory frame, respectively. These results supplement those of Saito *et al.* (Fig. 6 in Ref. 2). From an experimental point of view, the best way to obtain information about the symmetry modes is to perform Raman experiments on aligned isolated tubes or aligned bundles in backscattering configuration (see the Introduction). Note that in these latter experiments only the

dependence of the Raman intensity with θ_y can be measured. Consequently, in the following, we mainly discuss the VV and VH θ_y dependence of the Raman spectrum. For the VV configuration, the $A_1(A_{1g})$ and $E_1(E_{1g})$ tangential modes exhibit distinct behaviors with respect to the rotation angle. For all chiralities, the $A_1(A_{1g})$ mode has a minimum value at $\theta_y \approx 55^\circ$ while the $E_1(E_{1g})$ mode peaks at $\theta_y \approx 50^\circ$. Then, and despite the vicinity of their mode frequencies, the measurements in the VV configuration for the dependence of the Raman intensity with θ_y seem to be an efficient method to separate $A_1(A_{1g})$ and $E_1(E_{1g})$ modes in the TM bunch. In the VH configuration, the θ_y dependence of the $E_1(E_{1g})$ intensity peaks at a maximum at $\theta_y=0^\circ$ and $\theta_y=90^\circ$ and vanishes at $\theta_y=45^\circ$. The $A_1(A_{1g})$ and $E_2(E_{2g})$ modes have an inverse behavior. These dependences represent another method to separate the $A_1(A_{1g})$ and $E_1(E_{1g})$ modes in the TM bunch. Finally, the $E_2(E_{2g})$ modes present a significant intensity for $\theta_y=90^\circ$ in the VV configuration and can be preferentially measured in this configuration. The assignment

proposed by Jorio *et al.*¹⁴ from experiments on aligned nanotube bundles (see the Introduction), is in agreement with these predictions. Since the 1549 cm^{-1} and 1607 cm^{-1} lines only appear in their XX spectrum (VV configuration and $\theta_y=90^\circ$), they assign these peaks to $E_2(E_{2g})$ symmetry.¹⁴ However, in other experiments,^{10–12} the measured angular dependences of the TM intensity do not reflect the calculated behaviors of the different mode symmetries. In a nonresonant theory, the calculated VV intensity of $A(A_{1g})$ radial breathing modes increases with θ_y and peaks at a maximum at $\theta_y=90^\circ$, while the $E_1(E_{1g})$ RBM peaks at $\theta_y\approx 50^\circ$. These predictions contrast with the experimental behavior of the RBM intensity, which reaches a maximum when the light is polarized along the tube axis (ZZ, VV configuration and $\theta_y=0^\circ$), and is significantly reduced when the light (either incident or scattered) is polarized perpendicular to the tube axis (XX, VV configuration and $\theta_y=90^\circ$).^{10–12} This confirms that the polarization dependence of the Raman spectra is dominated by the resonant nature of the scattering process that breaks the symmetry selection rules. The sensitivity to mode symmetry is present in the polarized Raman spectra but it is of second order with respect to the resonant contribution. However, the mode symmetry can be detected from a detailed study of the polarization dependence of the different Raman bands that contribute to the TM bunch.^{14,30}

(iii) Finally, we investigated the chirality dependence of the polarized Raman spectrum in tangential mode region (Fig. 3). We calculated Raman spectra for five values of the chiral angle θ ($0^\circ, 10^\circ, 15^\circ, 20^\circ$ and 30°), associated with $(17,0)$, $(17,3)$, $(14,5)$, $(14,7)$, and $(10,10)$ nanotubes, respectively. The TM mode frequencies are only slightly sensitive to the tube diameter, except for the lowest-frequency mode for which a higher sensitivity is revealed by an oscillatory frequency behavior. This latter behavior corresponds to variations in the diameter of the selected tubes: 1.35 nm $(17,0)$, 1.48 nm $(17,3)$, 1.35 nm $(14,5)$, 1.47 nm $(14,7)$, and 1.37 nm $(10,10)$. Apart from that, the calculation results mainly illustrate the chirality dependence of the Raman spectra profile. For zigzag ($\theta=0^\circ$) and armchair ($\theta=30^\circ$) tubes, each polarized spectrum is featured by a single peak assigned to A_{1g} (ZZ), E_{1g} (ZX), and E_{2g} (YX) tangential modes, respectively. For each symmetry, let us call ω_z and ω_a the frequency of the zigzag and armchair TM mode, respectively. For each polarization, the increase of θ from 0° to 30° leads to the appearance of two peaks at frequencies close to ω_z and ω_a . The intensity of these peaks shifts from the one located around ω_z to that located around ω_a when increasing θ . For the armchair tube ($\theta=30^\circ$), a single peak located at ω_a has nonzero intensity. In agreement with direct calculations of TM frequencies,^{2,25,27} we found that the lowest-frequency component has E_{2g} symmetry for $(17,0)$ zigzag SWNT's, while for $(10,10)$ armchair SWNT's E_{2g} symmetry is found to be the highest-frequency mode. The separation of the two E_{2g} modes is around 20 cm^{-1} . In a nonresonant model and for chiral SWNT's, our calculations predict that six tangential modes have sufficient intensity to be detected in Raman experiments. All these results are in close agreement with recent calculations of chirality dependences of TM frequency and intensity using tight-binding

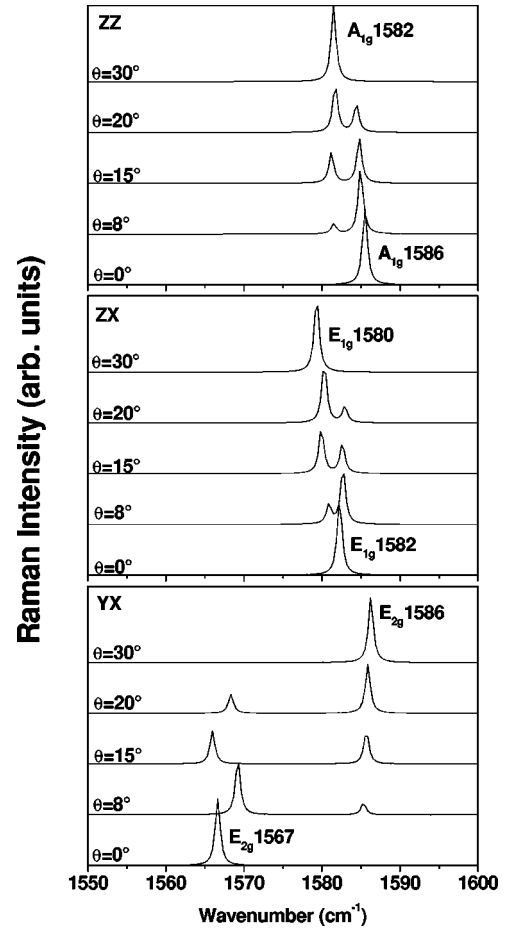


FIG. 3. Dependence of polarized Raman spectra of infinite crystals of SWNT's in the TM range as a function of the chiral angle θ .

molecular-dynamics methods and bond-polarization theory for the Raman tensor.²⁹ Recently, spectra of individual zigzag, chiral, and armchair SWNT's were identified in the TM region (Fig. 5 in Ref. 29). The experimental chirality dependence of the Raman profile is well described by the calculated θ dependence of the $A(A_{1g})$ and $E_1(E_{1g})$ modes reported in Fig. 3, and therefore the bands experimentally observed around 1575 and 1591 cm^{-1} in Ref. 29 are assigned to the superposition of $A(A_{1g})$ and $E_1(E_{1g})$ modes. For the chiral tube of Fig. 5 (middle) in Ref. 29, a comparison between the experimental relative intensity of the two bands and the calculated one (Fig. 3) gives a chiral angle θ of about 10° . Note, however that the resonance process mainly affects the relative intensity of the peaks of different symmetries. Indeed, contrary to our calculation that predicts close intensity of the two features for an average overall chiral SWNT's, it was experimentally found that the 1575 cm^{-1} band is always weaker than the 1590 cm^{-1} feature in a usual sample characterized by a large chirality dispersion.^{4,5,14}

B. Polarized Raman spectra of finite length SWNT's

Carbon nanotubes of finite length are important items in nanotube physics. Moreover, as-prepared nanotubes have

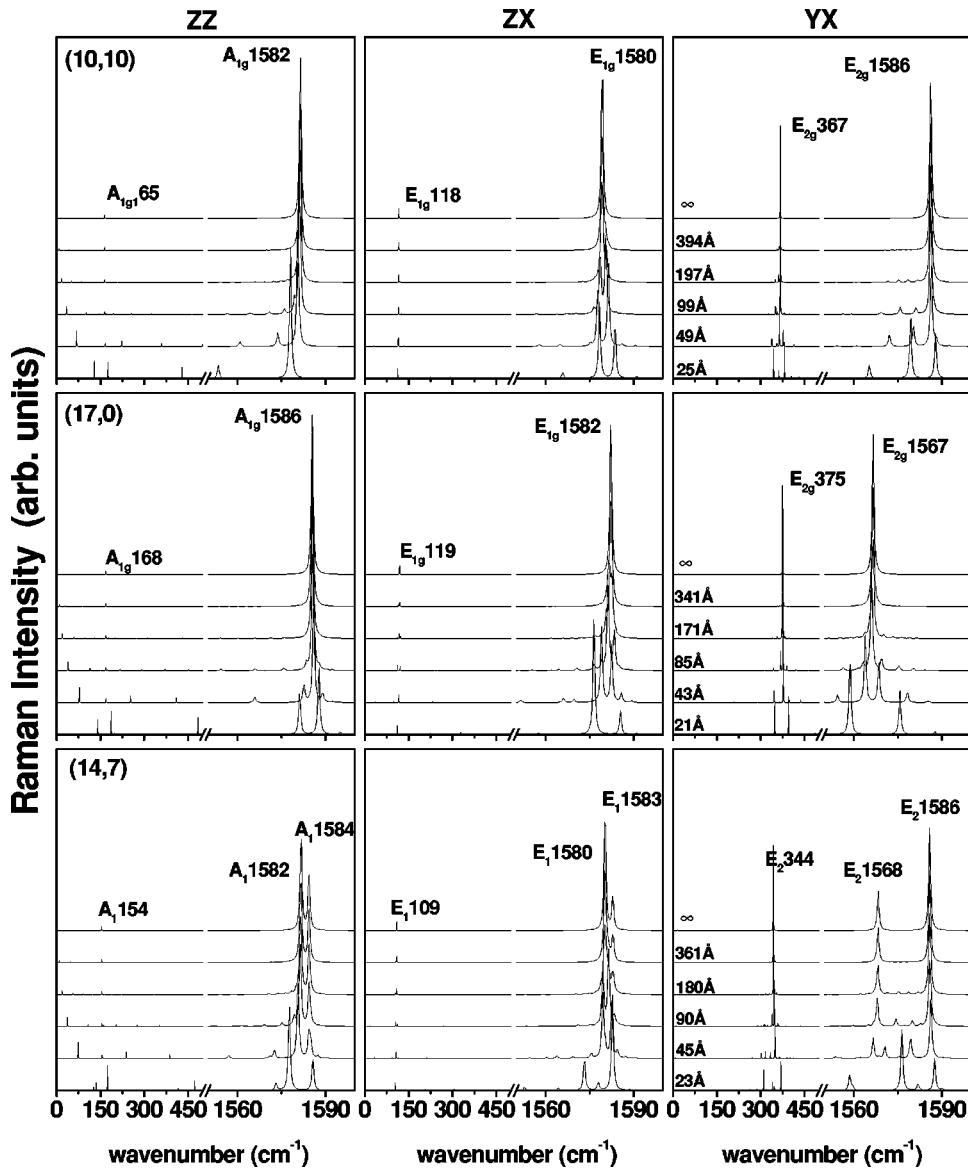


FIG. 4. Dependence of the polarized Raman spectrum as a function of the tube length: top, (10,10), middle (17,0), and bottom (14,7) SWNT's.

long but finite lengths on a micrometer scale, independently of the synthesis method. Moreover, cutting and opening of the tubes, e.g., for gas storage devices, contributes to shorten the tubes. The finite nature of the tube length was found to be an important feature for using nanotubes in industrial applications.³¹ It is thus of great interest to investigate the vibrational properties of nanotubes with a finite length. A few years ago, a theoretical study of finite-size effects on the Raman spectrum of (10,10) SWNT's was performed.⁸ With regard to the calculation method used in this previous approach, the investigation of finite-size effects was limited to a narrow length range (below 50 Å). The present work extends this previous analysis to a larger length range (from 20 to 850 Å), closer to reality, as well as to achiral and chiral tubes of different diameters. We calculate the Raman intensity of the finite length nanotube with open ends without any terminations.

A first illustration of our results is shown in Fig. 4. The dependences of $A(A_{1g})$, $E_1(E_{1g})$, and $E_2(E_{2g})$ polarized Raman spectra in the RBM and TM frequency range are dis-

played as a function of the nanotube length L for (10,10), (17,0), and (14,7) SWNT's. For all chiralities, we found an increase in the number of Raman active modes when the tube length decreases. Moreover, the relative intensities of the different peaks are significantly length dependent. For short tubes, $A(A_{1g})$ additional modes are observed at low frequency, and their frequencies significantly depend on the tube length (Fig. 4). A power law $\omega_0 \propto L^{-1}$ was found for the lowest-frequency mode. For short tubes, the profile of the TM bunch is more complex than in infinite SWNT's, especially for the $E_1(E_{1g})$ and $E_2(E_{2g})$ symmetries. We also found that the $A(A_{1g})$ modes of armchair tubes (zigzag) slightly up-shift (down-shift) when the length of the tubes increases (Fig. 4).

Figure 5 summarizes the dependence of all the Raman active mode frequencies with the tube length [only modes with an intensity greater than 10^{-3} times the intensity of the $A(A_{1g})$ TM are taken into account]. We observe that the most significant effect of finite size occurs in the intermediate range, 600–1100 cm^{-1} , where a large number of peaks

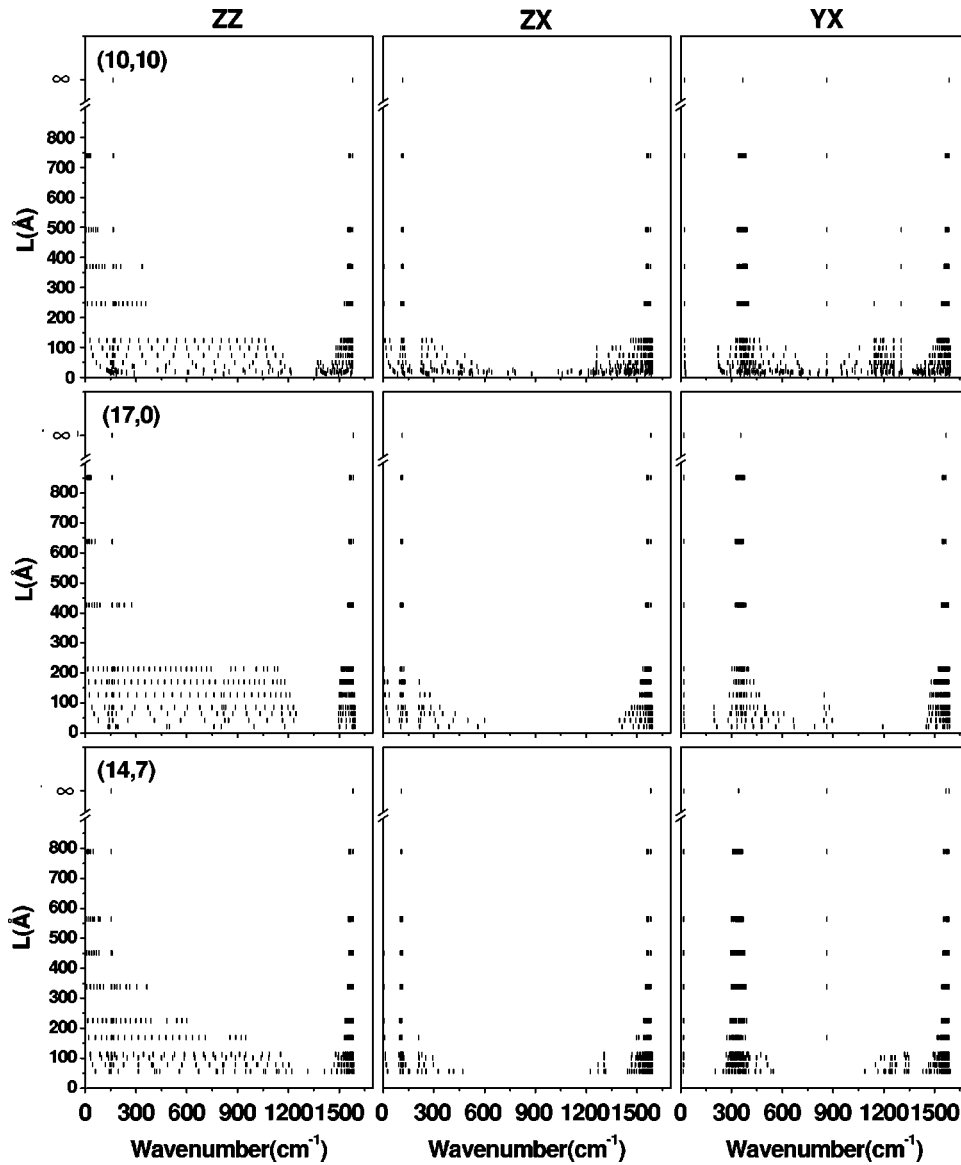


FIG. 5. Dependence of Raman-active mode frequencies as a function of the tube length for (10,10) (top), (17,0) (middle), and (14,7) (bottom) SWNT's.

are predicted to be Raman active, especially for $A(A_{1g})$ symmetry, and mainly for tube lengths below 200 Å. In the 1100–1300 cm^{-1} range, and mainly for armchair tubes, additional $E_2(E_{2g})$ modes are also calculated. Most of these peaks vanish for lengths > 500 Å.

Most VV and VH Raman experiments have been performed on unoriented samples.¹ To make the comparison with the experimental results more realistic, we thus used average overall nanotube orientations in the Raman spectra calculations (Fig. 6). Calculations were performed for five finite lengths, $L \approx 49, 98, 148, 197, 492$ Å for (10,10) SWNT's, $L \approx 43, 85, 170, 213, 511$ Å for the (17,0) SWNT's, $L \approx 23, 56, 113, 226, 564$ Å for (14,7) SWNT's, and for infinite SWNT's. The intermediate region is displayed in the inset of Fig. 6. First, it must be emphasized that, for a length greater than 500 Å (about 200 cells for an armchair tube), each polarized spectrum is close to that of an infinite tube. Then our calculations predict that the effects of the finite size of the tubes are only significant for short tubes. For raw SWNT's, which generally have lengths greater than 500 Å,

the RBM and TM experimental spectra can thus be interpreted under an infinite length approximation.

In the RBM range, independently of the tube length, the most important difference between VV and VH spectra is the complete disappearance of the $A(A_{1g})$ RBM in the VH configuration. By contrast, the $E_1(E_{1g})$ and $E_2(E_{2g})$ RBM modes appear in both spectra. In the TM range, and for long tubes, three (A_{1g}, E_{1g}, E_{2g}) modes for achiral tubes and six ($2A_{1g}, 2E_{1g}, 2E_{2g}$) modes for chiral tubes are present in both VV and VH configurations. Their intensity ratio is close of 0.8, i.e., significantly larger than the experimental value of about 0.4.³² The envelope of the TM is slightly dependent on the tube length, except for the smallest lengths (below 200 Å). In a nonresonant theory, the $E_1(E_{1g})$ tangential modes dominate the Raman spectrum in the TM range as well as in the VV configuration and in the VH configuration. However, the resonant nature of the Raman spectra of SWNT's must boost up the $A(A_{1g})$ modes intensity, which then becomes the most important contribution, especially in the VV configuration.

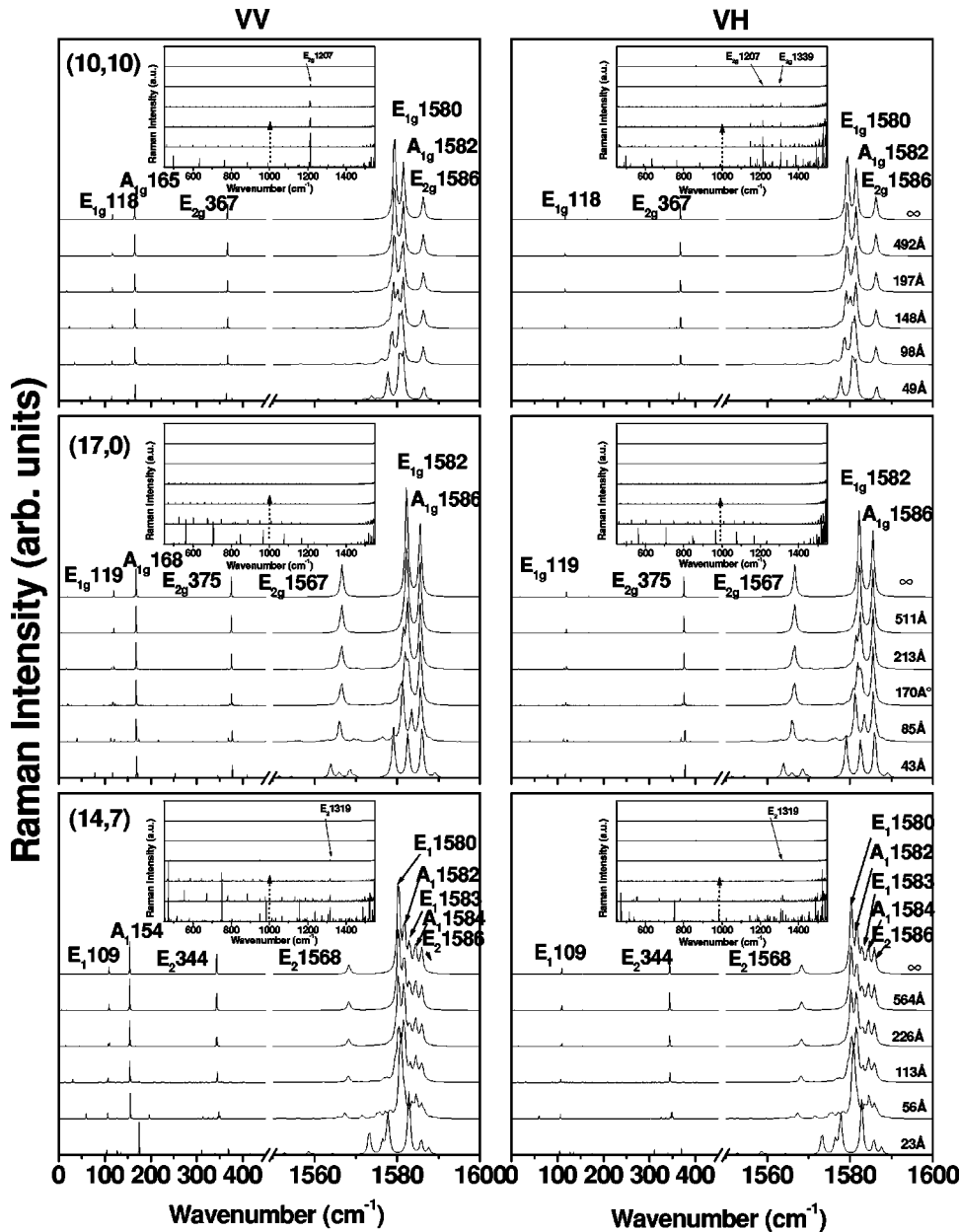


FIG. 6. The VV (left) and VH (right) calculated Raman spectra of unoriented samples of different lengths: (10,10) (top), (17,0) (middle), and (14,7) (bottom) SWNT's. In inset: the intermediate-frequency range.

Finally, in the intermediate-frequency region, and as previously discussed, the Raman activity strongly depends on the tube length. Very weak modes are observed around 865 cm⁻¹, independently of the tube length. In addition, weak lines also appear around $\omega \approx 1210$ cm⁻¹ and $\omega \approx 1340$ cm⁻¹ for armchair tubes and around $\omega \approx 1320$ cm⁻¹ for chiral tubes. However, the intensity of these modes decreases with the increase in the tube length, and vanishes for lengths larger than 300 Å. Even though this theoretical study sheds more light on the intermediate-frequency range, the calculated features of the Raman spectrum in this range do not explain the origin of the well-defined peaks measured between 700 cm⁻¹ and 850 cm⁻¹ in the Raman spectrum of SWNT's.⁹

Recently, a double-resonance Raman theory was developed to explain the dependence on the excitation energy of the disorder-induced band, the D band, and the second-order

feature, the G band, in graphite^{33,34} and SWNT's.^{35,36} We believe that the double-resonance theory, considering two-phonon (subtractive) processes, could also explain the behavior with respect to the excitation energy of Raman lines in the intermediate-frequency range.

IV. CONCLUSION

The spectral moments method was used to calculate the polarized nonresonant Raman spectra for achiral and chiral single-wall carbon nanotubes in a large diameter and length range. The chirality dependence of tangential modes was clearly observed, and recent experimental results are in agreement with these predictions.²⁹ The dependence of the Raman spectrum on the tube length was also calculated. The finite-size effects are shown to be significant only for short tubes ($L < 300$ Å). The main effect of the length shortening

is the appearance of additional peaks in the intermediate-frequency range $600\text{--}1300\text{ cm}^{-1}$. However, the frequency and intensity of these additional peaks cannot explain the experimental results in this range.⁹ The calculations revealed that, for a relatively short length of $\approx 500\text{ \AA}$, the spectra are similar to those of infinite tubes. This explains why no size effects have ever been clearly identified in Raman experiments on usual samples. The calculations also predict symmetry selection of the different modes in polarized Raman experiments. Experimentally, due to the resonant character of the Raman spectrum of nanotubes, the symmetry selection of

the different modes is not obvious.^{11,12} In order to improve the comparison between the calculations and experimental data, a numerical model accounting for both the symmetry of the modes and the resonant nature of the scattering process is currently under development.

ACKNOWLEDGMENTS

The computations were performed at CINES (Montpellier, France) on SP2 IBM computer. The work was supported by a CNRS-France/CNCPRST-Morocco agreement.

- ¹M.S. Dresselhaus and P.C. Eklund, *Adv. Phys.* **49**, 705 (2000), and references therein.
- ²R. Saito, T. Takeya, T. Kimura, G. Dresselhaus, and M.S. Dresselhaus, *Phys. Rev. B* **57**, 4145 (1998).
- ³H. Kataura, Y. Kumazawa, Y. Maniwa, I. Umezu, S. Suzuki, Y. Ohtsuka, and Y. Achiba, *Synth. Met.* **103**, 2555 (1999).
- ⁴M.A. Pimenta, A. Marucci, S.D.M. Brown, M.J. Matthews, A.M. Rao, P.C. Eklund, R.E. Smalley, G. Dresselhaus, and M.S. Dresselhaus, *J. Mater. Res.* **13**, 2396 (1998); M.A. Pimenta, A. Marucci, S.A. Empedocles, M.G. Bawendi, E.B. Hanlon, A.M. Rao, P.C. Eklund, R.E. Smalley, G. Dresselhaus, and M.S. Dresselhaus, *Phys. Rev. B* **58**, R16 016 (1998).
- ⁵L. Alvarez, A. Righi, T. Guillard, S. Rols, E. Anglaret, D. Laplaze, and J.-L. Sauvajol, *Chem. Phys. Lett.* **316**, 186 (2000).
- ⁶A.M. Rao, E. Richter, S. Bandow, B. Chase, P.C. Eklund, K.A. Williams, S. Fang, K.R. Subbaswamy, M. Menon, A. Thess, R.E. Smalley, G. Dresselhaus, and M.S. Dresselhaus, *Science* **275**, 187 (1997).
- ⁷E. Anglaret, N. Bendiab, T. Guillard, C. Journet, G. Flamant, D. Laplaze, P. Bernier, and J.L. Sauvajol, *Carbon* **36**, 1815 (1998).
- ⁸R. Saito, T. Takeya, T. Kimura, G. Dresselhaus, and M.S. Dresselhaus, *Phys. Rev. B* **59**, 2388 (1999).
- ⁹L. Alvarez, A. Righi, S. Rols, E. Anglaret, and J.-L. Sauvajol, *Chem. Phys. Lett.* **320**, 441 (2000).
- ¹⁰G.S. Duesberg, I. Loa, M. Burghard, K. Syassen, and S. Roth, *Phys. Rev. Lett.* **85**, 5436 (2000).
- ¹¹J. Hwang, H.H. Gommans, H. Tashiro, R. Haggemueller, K.I. Winey, J.E. Fischer, D.B. Tanner, and A.G. Rinzler, *Phys. Rev. B* **62**, R13 310 (2000).
- ¹²E. Anglaret, A. Righi, J.-L. Sauvajol, P. Bernier, B. Vigolo, and P. Poulin, *Phys. Rev. B*, (to be published).
- ¹³A.M. Rao, A. Jorio, M.A. Pimenta, M.S. Dantas, R. Saito, G. Dresselhaus, and M.S. Dresselhaus, *Phys. Rev. Lett.* **84**, 1820 (2000).
- ¹⁴A. Jorio, G. Dresselhaus, M.S. Dresselhaus, M. Souza, M.S.S. Dantas, M.A. Pimenta, A.M. Rao, R. Saito, C. Liu, and H.M. Cheng, *Phys. Rev. Lett.* **85**, 2617 (2000).
- ¹⁵P.H. Lambin and J.P. Gaspard, *Phys. Rev. B* **26**, 4356 (1982), and references therein.
- ¹⁶E. Jurczek, *Phys. Rev. B* **32**, 4208 (1985), and references therein.
- ¹⁷C. Benoit, G. Poussigues, and A. Assaf, *J. Phys.: Condens. Matter* **4**, 3153 (1992).
- ¹⁸C. Benoit, E. Royer, and G. Poussigues, *J. Phys.: Condens. Matter* **4**, 3125 (1992).
- ¹⁹A. Rahmani, C. Benoit, R. Jullien, G. Poussigues, and A. Sakout, *J. Phys.: Condens. Matter* **9**, 2149 (1997).
- ²⁰A. Rahmani, C. Benoit, R. Jullien, and G. Poussigues, *Philos. Mag. B* **77**, 421 (1998).
- ²¹G. Vilianni, R. Dell'Anna, O. Pilla, and M. Montagna, *Phys. Rev. B* **52**, 3346 (1995).
- ²²A. Rahmani, P. Jund, C. Benoit, and R. Jullien, *J. Phys.: Condens. Matter* **13**, 5413 (2001).
- ²³R.A. Jishi, L. Venkataraman, M.S. Dresselhaus, and G. Dresselhaus, *Chem. Phys. Lett.* **209**, 77 (1993).
- ²⁴S. Guha, J. Menéndez, J.B. Page, and G.B. Adams, *Phys. Rev. B* **53**, 13 106 (1996).
- ²⁵D. Kahn and J. Ping Lu, *Phys. Rev. B* **60**, 6535 (1999).
- ²⁶L. Henrard, E. Hernandez, P. Bernier, and A. Rubio, *Phys. Rev. B* **60**, R8521 (1999).
- ²⁷S. Rols, A. Righi, L. Alvarez, E. Anglaret, R. Almairac, C. Journet, P. Bernier, J.L. Sauvajol, A.M. Benito, W.K. Maser, E. Muñoz, M.T. Martinez, G.F. de la Fuente, A. Girard, and J.C. Ame-line, *Eur. Phys. J. B* **18**, 201 (2000).
- ²⁸A.C. Albrecht, *J. Chem. Phys.* **34**, 1476 (1961).
- ²⁹R. Saito, A. Jorio, J.H. Hafner, C.M. Lieber, M. Hunter, T. McClure, G. Dresselhaus, and M.S. Dresselhaus, *Phys. Rev. B* **64**, 085312 (2001).
- ³⁰Recent experiments on oriented SWNT's performed in our group have permitted to follow distinct angular dependences of the different components of the TM bunch in semiconducting SWNT's.
- ³¹S.J. Tans, R.M. Verschueren, and C. Dekker, *Nature (London)* **393**, 49 (1998).
- ³²K. Kneipp, A. Jorio, H. Kneipp, D.M. Brown, K. Shafer, J. Motz, R. Saito, G. Dresselhaus, and M.S. Dresselhaus, *Phys. Rev. B* **63**, 081401 (2001).
- ³³C. Thomsen and S. Reich, *Phys. Rev. Lett.* **85**, 5214 (2000).
- ³⁴R. Saito, A. Jorio, A.G. Souza Filho, G. Dresselhaus, M.S. Dresselhaus, and M.A. Pimenta, *Phys. Rev. Lett.* **88**, 027401 (2002).
- ³⁵J. Maultzsch, S. Reich, and C. Thomsen, *Phys. Rev. B* **64**, 121407 (2001).
- ³⁶A.G. Souza Filho, A. Jorio, A.K. Swan, M.S. Unlu, B.B. Goldberg, R. Saito, J.H. Hafner, C.M. Lieber, M.A. Pimenta, G. Dresselhaus, and M.S. Dresselhaus, *Phys. Rev. B* **65**, 085417 (2002).